Study of the annealing kinetic effect and implantation energy on phosphorus-implanted silicon wafers using spectroscopic ellipsometry

Emmanouil Lioudakis,[a] Constantinos Christofides, and Andreas Othonos
Photonics and Optoelectronics Research Laboratory, Department of Physics, University of Cyprus, P.O. Box 20537, 1678 Nicosia, Cyprus

(Received 6 December 2005; accepted 4 April 2006; published online 26 June 2006)

In this work, we have studied the changes in the optical properties on crystalline silicon implanted wafers (1×10^{13}–1×10^{16} P^+/cm^2) using an extensive ellipsometric analysis. The effects of implantation energy (20–180 KeV) and subsequent isochronical annealing temperature (300–1100 °C) on the electronic band structure of material are investigated. The evolution of pseudodielectric functions is studied using a temperature dependent multilayer model for each implantation dose and energy. The temperature evolution of integrated damage depth profile for each wafer is presented depicting the amorphous/crystalline transition temperatures. Finally, the critical implantation dose and energy of crystalline to amorphous silicon phase are given. © *2006 American Institute of Physics*. [DOI: 10.1063/1.2207688]

I. INTRODUCTION

The crystalline silicon properties combined with its abundance in nature have given it a unique position in the fabrication of miniaturized devices that is not likely to be challenged soon. Ion implantation is routinely used in silicon devices manufacturing to dope the active regions of transistors. As the minimum feature size of integrated circuits has decreased over the years, the implant energies used by the semiconductor industry have changed. The depth distribution of the implanted ions after they come to rest, the damage created in the lattice by the ions and energetic recoils, and the relocation of dopant atoms by diffusion during high temperature annealing are all valuable quantities required in manufacturing.[1,2]

There have been a number of experimental techniques (such as Rutherford backscattering, cross-section transmission electron microscopy, and infrared spectroscopy) employed in studies of the nature of the damage and amorphization.[3] Furthermore, a lot of work has been reported describing the optical properties of ion-implanted (Ar^+, As^+, Si^+, and P^+) Si layers studied by spectroscopic ellipsometry (SE).[4–6] SE technique is able to detect and characterize the degree of crystallinity in buried layers, besides depth profiling the sample.[7,8] The redistribution of the impurity atoms (vacancies, interstitial pairs, etc,) and the annihilation of the damaged material due to the rapid thermally annealing have also been studied.[9]

However, although a better understanding has been gained in the area of Si ion-implantation technology, little is known about the influence of implantation energy on the optical properties (dielectric functions) as well as the effects of subsequent isochronical annealing temperature. In this work, we report the changes of the optical properties of implanted Si wafers employing a multiwavelength spectroscopic ellipsometer over an energy range of 1.5–6 eV. The samples used in this work are crystalline silicon wafers implanted at different doses (1×10^{13}–1×10^{16} P^+/cm^2, with 150 KeV) and different implantation energies (20–180 keV, with 5×10^{14} P^+/cm^2). The phosphorous implantation was performed through a thin oxide layer (~2 nm) at room temperature. Some of the samples were then annealed isochronically at various temperatures ranging from 300–1100 °C for 1 h in an inert nitrogen atmosphere. We should point out that although a broad range of phosphorous implantation dose is used in this work the structural changes and the optical properties of these nonannealed wafers are not the subject of our study.

II. RESULTS AND DISCUSSION

It is known that the influence of implantation dose in the structural properties of silicon wafers reveals changes in the electronic energy-band structure and, therefore, in the optical properties of this material. Figure 1 shows the real and the imaginary part of pseudodielectric functions (ε_1 and ε_2) of nonannealed silicon wafers for all implantation doses under investigation in this work. It is clearly evident from ellipsometric data that the implantation dose plays a crucial role to the optical properties of material.

The pseudodielectric functions appear to have two distinct behaviors: (i) for low implantation doses, the optical properties of wafers are close to Si nonimplanted, nonannealed reference sample; (ii) with increasing the dose, the pseudodielectric functions exhibit different line shapes (these line shapes are typical of amorphous tetrahedrally bonded material)[11] accompanied with oscillations for low energies. It is interesting to point out that the ellipsometric data reveal the reported amorphous/crystalline phase transition between 5×10^{14} and 1×10^{15} P^+/cm^2.[12] With increasing the implantation dose, the critical points (CPs) disappear due to the breakdown of lattice periodicity providing a single-broad peak (at 3.25 eV). Furthermore, we observe that the CPs (transition energies) are reduced in amplitude (with different rate), are broadened, and are moved to lower energies. The

[a]Author to whom correspondence should be addressed; FAX: +35722892821; electronic mail: mlioud@ucy.ac.cy

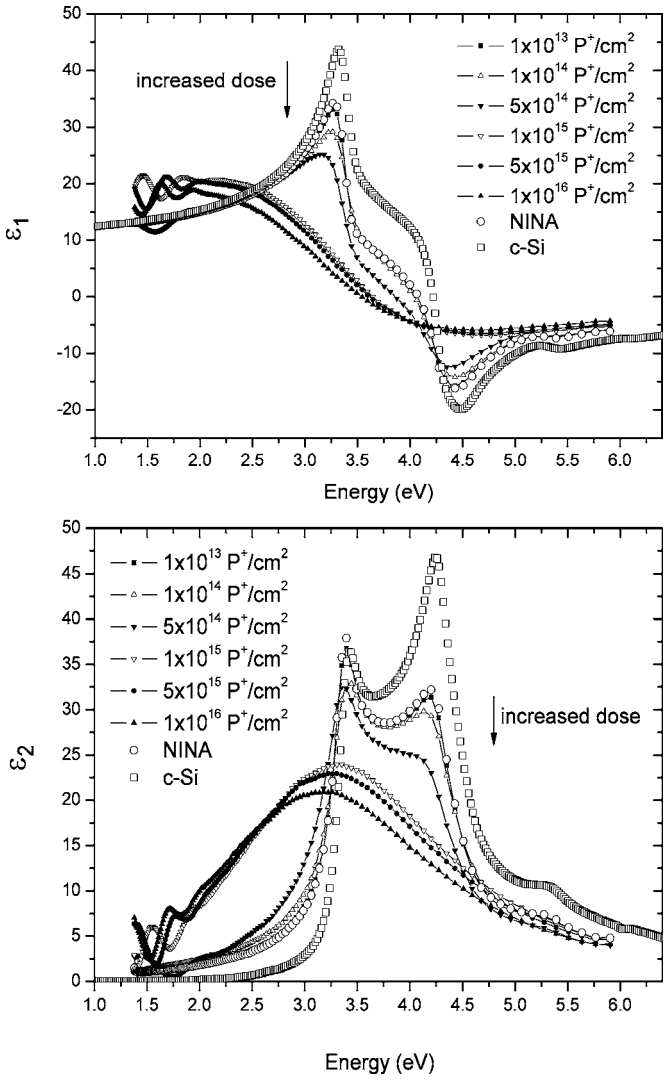

FIG. 1. Pseudodielectric functions of Si wafers at different implantation doses (1×10^{13}–1×10^{16} P^+/cm^2), with constant implantation energy of 150 KeV. For comparison the $\varepsilon(E)$ spectra for nonimplanted, nonannealed (NINA) reference and crystalline silicon (*c*-Si) samples (Ref. 10) are shown (points).

small oscillations, which are observed for low energies, may be attributed to the multiple reflections from the inner boundaries of silicon phases (*c*-Si, *a*-Si, etc.). We should point out that the different line shapes of dielectric functions of reference sample from that of crystalline silicon is due to the native silicon dioxide layer.[13]

In order to investigate the dynamic of isochronical annealing temperature on the optical properties of these wafers, a structural multilayer model was utilized. This model is based on Monte Carlo simulations (TRIM calculations) of penetration of phosphorous ions in silicon.[14] The damaged depth for each wafer $d_T=0.4$ μm is divided into m sublayers with equal thickness $z_m=d_T/m$. Each sublayer has its own complex dielectric function which is represented using Bruggeman effective medium approximation (BEMA).[15] The damage level of each wafer is calculated by an upgraded damage depth profile function,[16,17]

$$D(z_m) = 1 - \exp\{-f(T)\exp[-[z_m - \mu(\mathrm{T})]^2 / 2\sigma^2(T)\},$$

where $f(T)$ is the fraction of amorphous phase (*a*-Si) which is depended on the implantation dose, and $\mu(T)$ and $\sigma(T)$ are the estimated mean value and standard deviation of the density of ion-induced vacancies from TRIM calculations. We should point out that the parameters f, μ, and σ of our model depend on the annealing temperature and the density of ion-induced vacancies refers to vacancy-interstitial pairs (Frenkel pairs).[18] It is known that the amorphization in crystalline silicon is much more complex than simply vacancy formation. It entails formation of Frenkel pairs, point defects, and amorphous nanoclusters[19] where collision cascades are located.

The utilized fitting process in this work is the nonlinear Levenberg-Marquardt regression method and the error function is defined by the formula,[20]

$$\chi = \left\{ \frac{1}{(N-P-1)} \sum_{j=1}^{N} [(\cos\Delta_j^{\mathrm{meas}} - \cos\Delta_j^{\mathrm{regr}})^2 + (\tan\Psi_j^{\mathrm{meas}} - \tan\Psi_j^{\mathrm{regr}})^2] \right\}^{1/2},$$

where N is the number of independently measured values corresponding to different wavelengths and P is the number of unknown model parameters. (Here "meas" and "regr" refer to the measured and regression values, respectively).

Using the above ellipsometric analysis, the regression results for the nonannealed and annealed wafers fit well to the experimental data for all doses under investigation in this work. In Fig. 2 we present some typical fitting curves with the solid lines throughout the experimental ellipsometric data (points) for the nonannealed and annealed wafers using $m=5$ sublayers. We note that with increasing annealing temperature the damage depth profile function $D(z_m)$ is reduced approaching zero. The sublayers described initially with *a*-Si $[D(z_m)=1]$ for the nonannealed wafers are replaced with mixture layers (*c*-Si/*a*-Si) due to increasing of annealing temperature (gradual recrystallization).

The optical properties for all implanted wafers were investigated using the above analysis. Figures 3(a) and 3(b) show the evolution of pseudodielectric functions due to the isochronical temperature annealing of highly implanted wafer. With increasing the annealing temperature the wafer almost recovers the initial structure (see the reference sample). We observe a transition temperature (700–800 °C) where the wafer appears an abrupt long-range ordering due to the recovery of lattice periodicity. After this temperature the damaged regions of material are gradually recrystallized. We should point out that the integrated damage depth profile function of our multilayer model $\int_0^{d_T} D(z)dz$ exhibits an abrupt drop for all implanted wafers for (700–800 °C) depicting the generality of transition temperature [Fig. 3(c)].

It is interesting to note that for wafers implanted at high doses the integrated damage depth profile is similar, depicting the saturation effects. Furthermore, at annealing temperature of 800 °C the ellipsometric analysis of highly implanted wafer has depicted a buried end of range defect zone (~2 nm) attributed to the remained dislocation lines and loops at this temperature. This observation has already been verified from cross-section transmission electron micrographs in the same set of samples.[21] Finally, partial damage

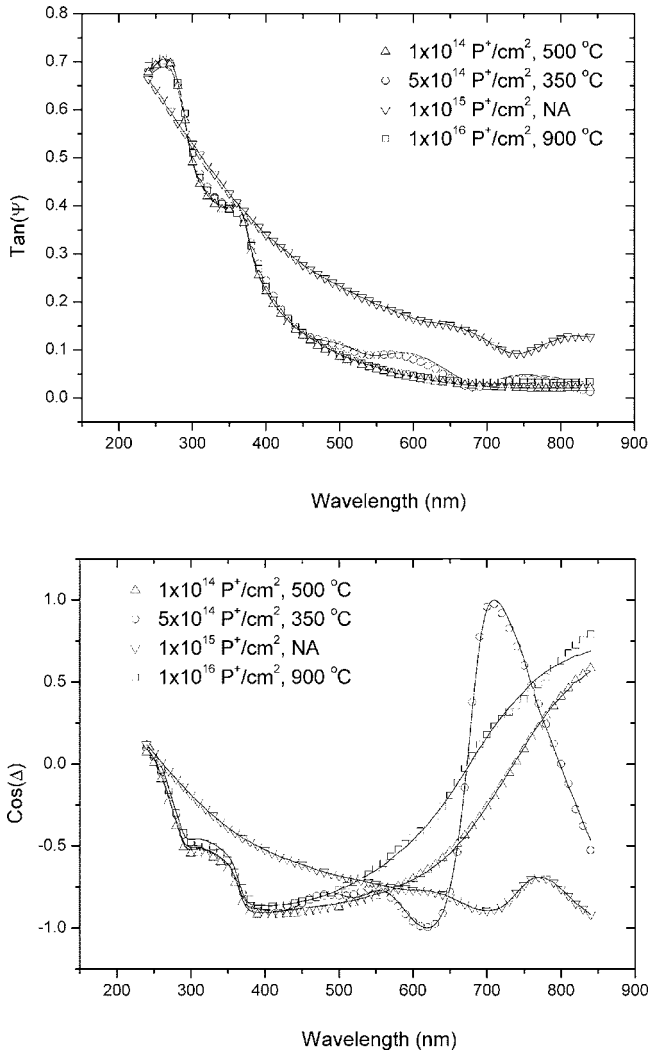

FIG. 2. Fitting curves (solid lines) throughout the experimental ellipsometric data (points) using the above analysis for various wafers at different implantation doses and annealing temperatures.

in low implanted samples is minor and even low-temperature annealing restores the wafers back to their crystalline silicon structure.

In order to investigate the influence of implantation energy on the optical properties of silicon wafers as well as the subsequent isochronical annealing temperature, we applied our ellipsometric analysis on the second set of wafers. Figures 4(a) and 4(b) show the pseudodielectric functions of the nonannealed silicon wafers for different implantation energies. With increasing the implantation energy the bombarded phosphorous ions penetrate deeper to the silicon target causing larger damage [Fig. 4(c)]. This is also provided from the generated inner boundaries inside the silicon target at different depths from the surface causing oscillations in the pseudodielectric functions of material for low energies.

As seen from the above figure, the implantation energy is a key contributing factor to doping the silicon wafers. The optical properties (dielectric functions) in these wafers and the ion-induced damaged regions appear to have a more complex behavior. Specifically, the ion-implantation damage to the wafers is apparent even at low implantation energy (as low as 20 KeV). With increasing the implantation energy the

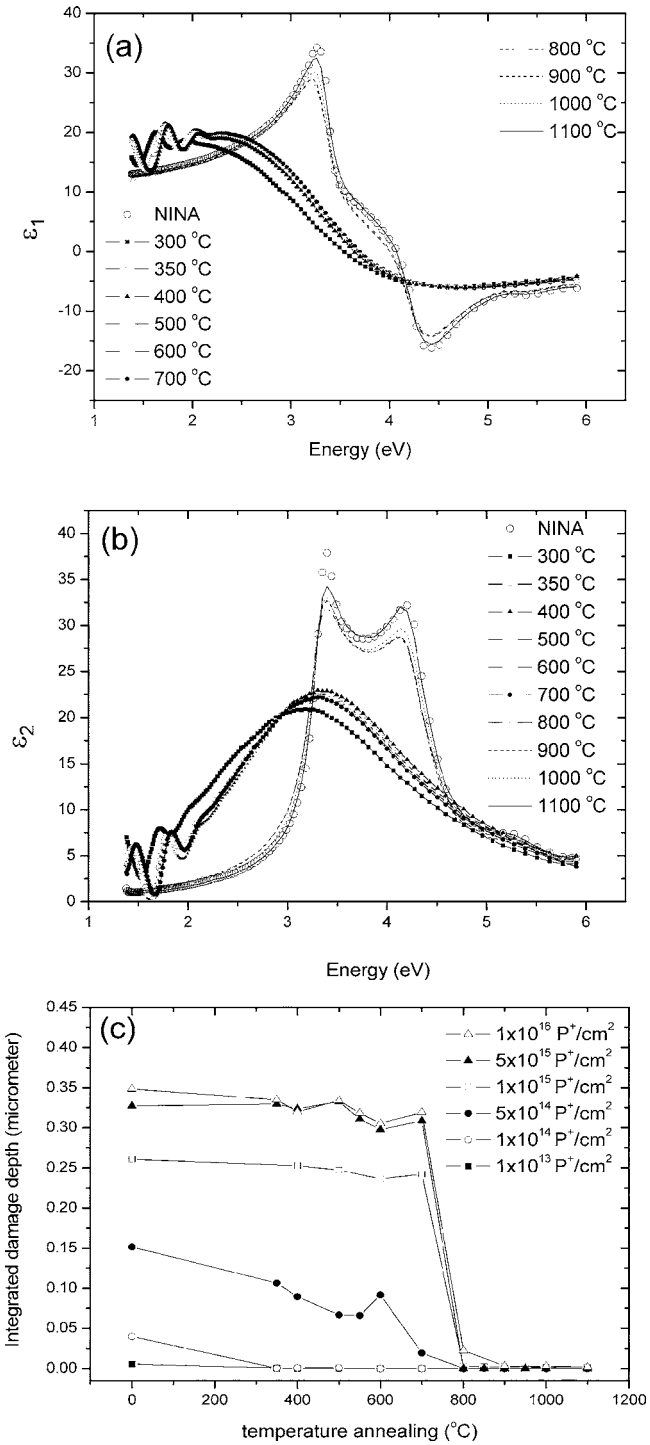

FIG. 3. [(a) and (b)] Evolution of pseudodielectric functions of highly implanted Si wafer due to the isochronical annealing temperature. For comparison the $\varepsilon(E)$ spectra for nonimplanted, nonannealed (NINA) reference sample is shown (points). (c) shows the dynamic of isochronical annealing temperature on the damage depth profile for all implanted wafers.

transition energy is moved to higher energies. After the critical implantation energy (100 KeV) the pseudodielectric functions approach the line shapes of nonimplanted, nonannealed reference sample generating three critical points (as exactly in the crystalline silicon).[10] We should point out that these results are coincident with the TRIM calculations with various implantation energies and constant doping concentration of 5×10^{14} P$^+$/cm^2 [Fig. 4(c)]. We note that for all wa-

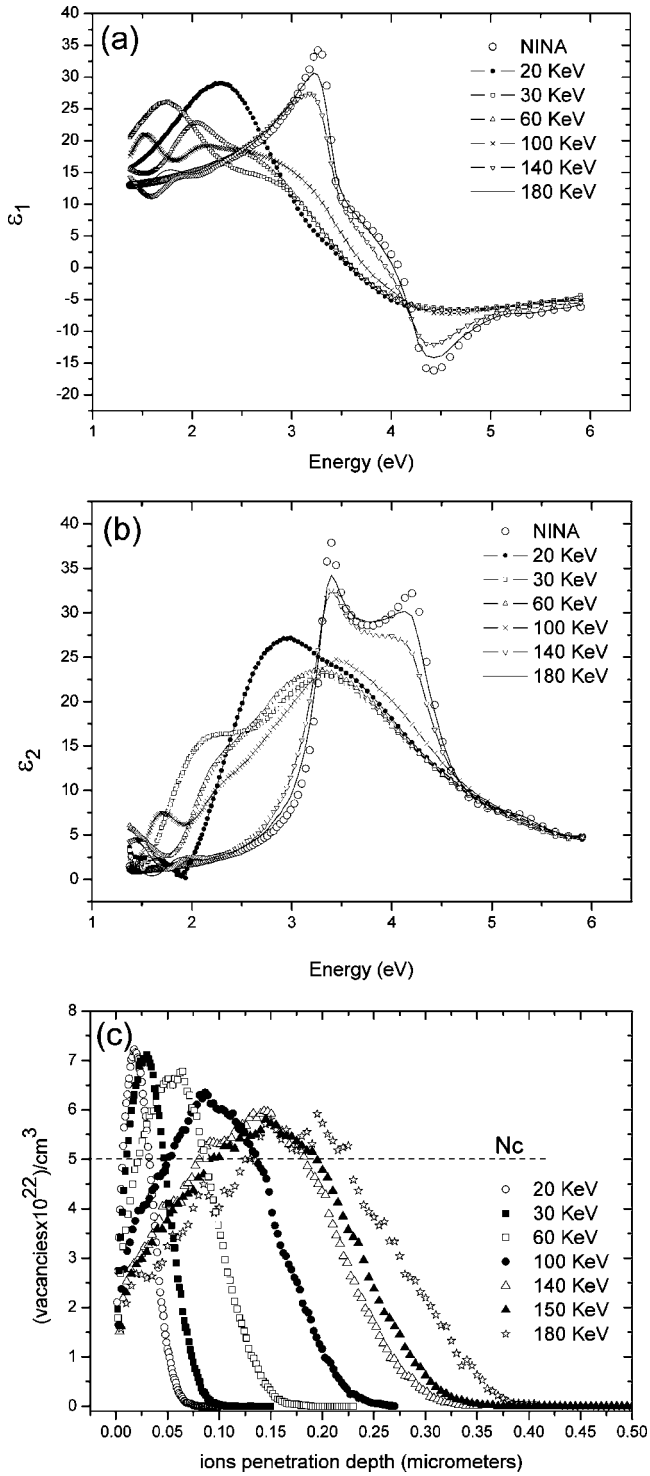

FIG. 4. [(a) and (b)] Pseudodielectric functions of Si wafers at different implantation energies (20–180 KeV), with constant implantation dose of 5×10^{14} P^+/cm^2. For comparison the $\varepsilon(E)$ spectra for nonimplanted, nonannealed (NINA) reference sample is shown (points). (c) shows the reconstruction of the damage depth profile using TRIM calculations of the phosphorous ion implantation in silicon at various implantation energies. The horizontal line represented by N_c corresponds to the critical amorphization density.

fers implanted at different energies the density of ion-induced vacancies is higher than the critical amorphization density ($N_c=5\times10^{22}$ cm^{-3}) and is gradually decreased with increasing the implantation energy. In addition, the penetration depth d_T increases generating larger damaged regions inside the silicon target.

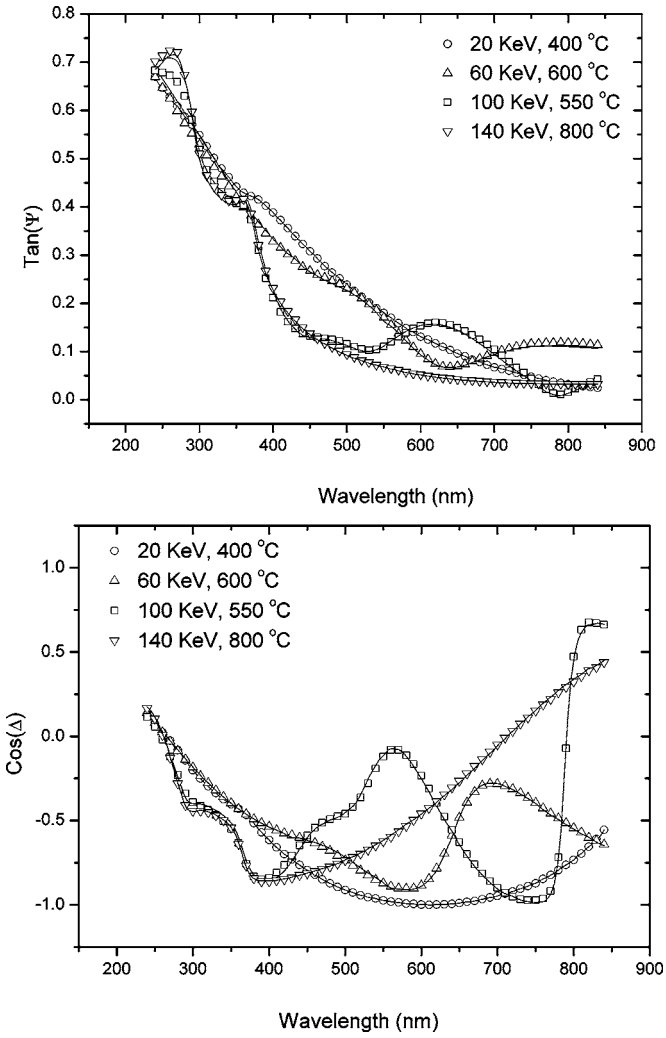

FIG. 5. Fitting curves (solid lines) throughout the experimental ellipsometric data (points) using the above analysis for various wafers at different implantation energies and annealing temperatures.

Our structural multilayer model was suitably modified in order to represent the structural changes of the nonannealed and annealed wafers of this set. The parameters f, μ, and σ are now depended on the implantation energies as well as the isochronical annealing temperature. As seen from Fig. 4(c) the mean value of ion-induced damage profile is shifted to higher values and the standard deviation is broadened with increasing the implantation energy. Furthermore, the fraction of amorphous phase gradually decreases with increasing the implantation energy.

Using the above multilayer model, the regression results for the nonannealed and annealed wafers fit well to the experimental data for all implantation energies. In Fig. 5 we present some typical fitting curves with the solid lines throughout the experimental ellipsometric data (points) for the nonannealed and annealed wafers using $m=5$ sublayers. We should point out that due to the change of damaged depth d_T the spatial resolution of our model z_m also change. Due to the gradually recrystallization of the wafers, some damaged regions were eliminated $[D(z_m)=0]$ or the concentration of amorphous to crystalline silicon in mixture layers is decreased and consequently the mixture layers were replaced by the crystalline silicon.

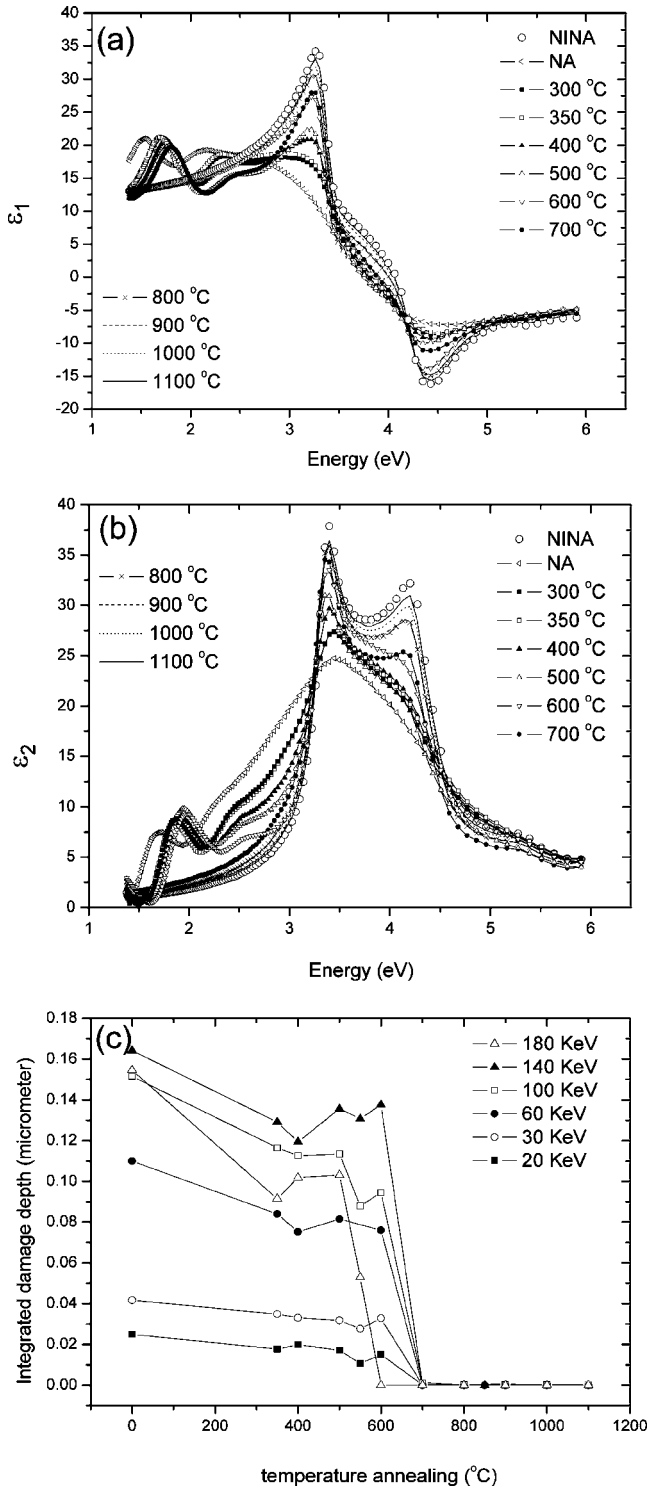

FIG. 6. [(a) and (b)] Evolution of pseudodielectric functions of Si wafer with 5×10^{14} P^+/cm^2 and 100 KeV at various annealing temperatures ranging from 300 to 1100 °C. The open circles show the nonimplanted, nonannealed (NINA) reference sample for comparison purpose. (c) shows the dynamic of isochronical annealing temperature on the damage depth profile for all implantation energies.

The optical properties for all implantation energies of this work were investigated using the above analysis. In Figs. 6(a) and 6(b) we show a typical evolution of the pseudodielectric functions due to the dynamic of isochronical annealing temperature. The optical properties of wafer with 5×10^{14} P^+/cm^2 and 100 KeV gradually change due to the annealing temperature ranging from 300 to 1100 °C. We should point out that this wafer appears to have an amorphous/crystalline phase transition between the temperatures (600–700 °C). With increasing the annealing temperature above this threshold the peaks of transition energies are enhanced approaching the pseudodielectric functions of nonimplanted, nonannealed Si reference sample (points).

As seen from these results the isochronical annealing temperature effects significant to the structural changes of wafers. These changes modify the electronic band structure of material causing changes in the optical properties. Figure 6(c) presents the dynamic of annealing on the integrated damage depth profile for each wafer of the second set. We observe that all wafers are gradually recrystallized and an abrupt drop of the integrated damage profile is appeared between 600 and 700 °C.[12] The only noticeable change is the transition temperature of highest implantation energy (500–600 °C). The integrated damaged depth of silicon gradually increases up to 140 KeV and begins to drop with increasing the implantation energy. We believe that this is attributed to two reasons: (a) although the ions penetrate deeper to the highest implanted wafer with increasing the implantation energy, the ion-induced density of vacancies gradually decreases compensating the formation of damaged regions; (b) with increasing the implantation energy of 180 KeV, the bombarded ions increase the lattice temperature results self-annealing phenomena.[20]

III. CONCLUSION

In conclusion, we have used ellipsometric analysis for studying the changes in optical properties of implanted silicon wafers. We have presented the effects of ion implantation (different doses and energies) on the pseudodielectric functions of material. We should point out that the implantation parameters are key contributing factors in the structural changes of material and consequently in optical properties. Furthermore, we have found that the subsequent isochronical annealing temperature tailors the electronic band structure (pseudodielectric functions) of implanted silicon wafers causing gradual recrystallization.

Especially, we have constructed optical/structural multilayer model for both sets of wafers, where the BEMA was used in obtaining the various mixture profiles of silicon phases. The accuracy of our model depends on the number m of sublayers increasing the computation time. The parameters f, μ, and σ of our model were temperature dependent to explain the ellipsometric data for all annealing temperatures under investigation in this work. Our ellipsometric regression procedure provides valuable information (integrated damage depth profile, amorphous/crystalline transition temperatures, and optical properties) on the dynamics of isochronical annealing and implantation energies, in these crystalline silicon wafers. Finally, we should point out that self-annealing effect plays a crucial role in the optical properties of wafers with high implantation dose and energy.

[1] J. L. Benton, S. Libertino, P. Kringhoj, D. J. Eaglesham, M. Poate, and S. Coffa, J. Appl. Phys. **82**, 120 (1997).
[2] C. Christofides and G. Ghibaudo, *Effects of Disorder and Defects in Ion-*

Implanted Semiconductors: Optical and Photothermal Characterization, Semiconductors and Semimetals, Vol. 46, (Academic, New York, 1997).
[3]H. Wong, J. Lou, N. W. Cheung, E. P. Kvam, K. M. Yu, D. A. Olson, and J. Washburn, Appl. Phys. Lett. **57**, 798 (1990).
[4]K. Kurihara, S. Hikino, and S. Adachi, J. Appl. Phys. **96**, 3247 (2004).
[5]K. Tsunoda, S. Adachi, and M. Takahashi, J. Appl. Phys. **91**, 2936 (2002).
[6]P. K. Giri, S. Tripurasundari, G. Raghavan, B. K. Panigrahi, and P. Magudapathy, J. Appl. Phys. **90**, 659 (2001).
[7]H. Mori, S. Adachi, and M. Takahashi, J. Appl. Phys. **90**, 87 (2001).
[8]E. Lioudakis, A. G. Nassiopoulou, and A. Othonos, Thin Solid Films **496**, 253 (2006).
[9]S. Hikino and S. Adachi, J. Phys. D **37**, 1617 (2004).
[10]R. Hull, *Properties of Crystalline Silicon* (INSPEC, London, United Kingdom, 1999).
[11]S. Adachi, Phys. Rev. B **43**, 12316 (1991).
[12]A. Othonos, C. Christofides, and A. Mandelis, Appl. Phys. Lett. **69**, 821 (1996).
[13]G. E. Jellison, Jr., S. P. Withrow, J. W. McCamy, J. D. Budai, D. Lubben, and M. J. Godbole, Phys. Rev. B **52**, 14607 (1995).
[14]J. F. Ziegler, J. P. Biersack, and U. Littmark, *The Stopping Range of Ions in Solids* (Pergamon, Tarrytown, NY, 1985); TRIM software, SRIM-version 2003.26: http://www.srim.org/.
[15]D. E. Aspnes, Thin Solid Films **81**, 249 (1981).
[16]M. Fried, T. Lohner, W. A. M. Aarnink, L. J. Hanekamp, and A. van Silfhout, J. Appl. Phys. **71**, 2835 (1992).
[17]M. Fried and L. Rédei, Thin Solid Films **364**, 64 (2000).
[18]W. J. Weber, Nucl. Instrum. Methods Phys. Res. B **166–167**, 98 (2000).
[19]W. J. Weber, F. Gao, R. Devanathan, W. Jiang, and C. M. Wang, Nucl. Instrum. Methods Phys. Res. B **216**, 25 (2004).
[20]R. Azzam and N. Bashara, *Ellipsometry and Polarized Light* (North-Holland, Amsterdam, 1977).
[21]A. Othonos and C. Christofides, Phys. Rev. B **66**, 085206 (2002).